Triple mirror assembly in the GRACE Follow-On laser ranging interferometer

Klaus Abich,[1,*] Andreas Baatzsch,[2] Christina Bogan[3,†] Claus Braxmaier[1,‡] Karsten Danzmann[3]
Germán Fernández Barranco,[3] Martin Gohlke[1,§] Gerhard Heinzel[3] Mark Herding,[2]
Martin Hinz[4] Marina Kaufer,[2] Alexander Koch[3,‖] Thomas Leikert[4] Christoph Mahrdt[3,¶]
Malte Misfeldt[3,**] Vitali Müller,[3] Kolja Nicklaus[2] Jens Reiche[3] Josep Sanjuan[1,††]
Daniel Schütze[3,‡‡] Gunnar Stede,[3,§§] Kai Voss,[2] Henry Wegener[3] and Marcus Zimmermann[4]

[1]*DLR Institut für Raumfahrtsysteme*, Robert-Hooke-Str. 7, 28359 Bremen, Germany
[2]*SpaceTech GmbH*, Seelbachstrasse 13, 88090 Immenstaad, Germany
[3]*Max-Planck-Institut für Gravitationsphysik (Albert-Einstein-Institut)* and *Institut für Gravitationsphysik of Leibniz Universität Hannover*, Callinstrasse 38, 30167 Hannover, Germany
[4]*Hensoldt Optronics GmbH*, Carl-Zeiss-Straße 22, 73447 Oberkochen, Germany

The Gravity Recovery And Climate Experiment (GRACE) Follow-On mission was launched on May 22, 2018, to continue monitoring changes in the gravity field of the Earth by measuring distance variations between two spacecraft that fly 200 km apart in a low-Earth polar orbit. The laser ranging interferometer (LRI), a technology demonstrator onboard GRACE Follow-On, is the first of its kind to perform inter-spacecraft ranging measurements and has shown noise levels of $1 \, \mathrm{nm}/\sqrt{\mathrm{Hz}}$ at 100 mHz and $200 \, \mathrm{pm}/\sqrt{\mathrm{Hz}}$ at 5 Hz. Its development was shared between parties in Germany and the United States. A key optical component for the LRI's success is the triple mirror assembly (TMA), which acts as a corner-cube retroreflector and enables the laser link between the two spacecraft. This paper presents the TMA design and characterization from the unit level to measurements in orbit. The in-orbit measurements furthermore provide the far-field intensity distribution of the Gaussian beams exchanged between the spacecraft after traveling 200 km. We address lessons learned that have influenced the design of the next generations of the LRI.

I. INTRODUCTION

The US-German Gravity Recovery And Climate Experiment (GRACE, 2002–2017 [1,2]) and GRACE Follow-On

———————

*Now at eleQtron GmbH, Hamburg, Germany.

†Now at Volkswagen AG, Wolfsburg, Germany.

‡Now at DLR Institut für Quantentechnologien, Ulm, Germany and Universität Ulm, Institute of Microelectronics, Ulm, Germany.

§Now at DLR Institut für Quantentechnologien, Ulm, Germany.

‖Now at DLR Institut für Satellitengeodäsie und Inertialsensorik, Hannover, Germany.

¶Now at Siemens Mobility GmbH, Braunschweig, Germany.

**Contact author: malte.misfeldt@aei.mpg.de

††Now at Texas A&M University, USA.

‡‡Now at OHB-System AG, Bremen, Germany.

§§Now at Schule im Allertal, Winsen (Aller), Germany.

(2018–now [3,4]) missions map Earth's gravity field with unprecedented accuracy and time resolution. Such observations have proven crucial for a better understanding of the Earth's dynamics by disciplines such as climate research, hydrology, geology, and oceanography. Both missions consist of two almost identical satellites in a near-polar low-Earth orbit, separated by 220 ± 50 km. That distance varies slightly due to the differential gravitational pull at one instance of time. GRACE used a microwave instrument (MWI) [5] to measure these distance changes between two spacecraft (SC) at the micrometer level by means of dual one-way ranging, which, together with accelerometer data and GPS orbit determination, allowed the reconstruction of the gravity field of the Earth on a monthly basis. Owing to the success of GRACE, the need to keep monitoring the Earth's gravity field beyond the mission's lifetime became clear. GRACE's decommissioning occurred in October 2017 after it had more than tripled its design lifetime. GRACE Follow-On [3,6] was launched on May 22, 2018, keeping the MWI as the main ranging instrument. Additionally, the laser ranging interferometer (LRI) [7,8], was added to the mission as a technology demonstrator, with the goals of
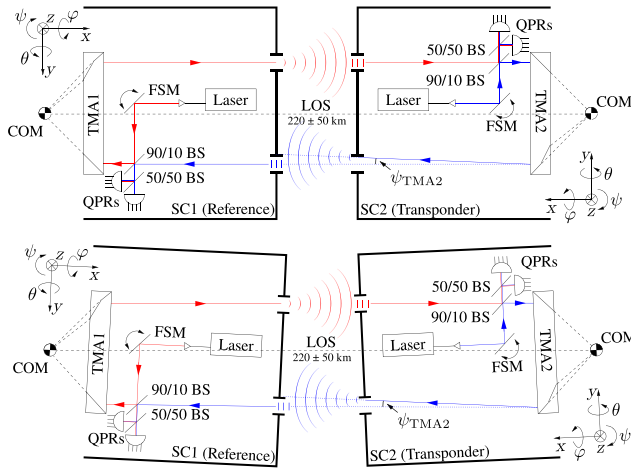
FIG. 1. Simplified LRI layout. Top: SC and LOS perfectly aligned; TMA1 is ideal, TMA2 has a coalignment error in yaw, ψ_{TMA2}. The nonideal TMA2 introduces a misalignment of the transmitted beam with respect to the LOS or nominal direction shown as a dotted vector, which reduces the power received by the far SC. Bottom: Both SC are rotated with respect to the LOS. The SC rotations are measured by the QPRs using DWS and corrected by steering the local beam using the FSM. LRI, laser ranging interferometer; SC, spacecraft; TMA, triple mirror assembly; BS, beam splitter; COM, center of mass; LOS, line of sight; QPR, quadrant photoreceiver; FSM, fast steering mirror; DWS, differential wave-front sensing; θ, pitch; ψ, yaw; ϕ, roll.

measuring ranging variations between the SC with noise levels below $80\,\text{nm}/\sqrt{\text{Hz}}$ and of paving the way for future laser-interferometric Earth-science missions GRACE-C and ESAs' next generation gravity mission (NGGM) [9,10] and gravitational wave observatories in space such as the Laser Interferometer Space Antenna [11].

The LRI is the first interspacecraft laser interferometer and has been measuring distance variations between the SC at the level of $1\,\text{nm}/\sqrt{\text{Hz}}$ for Fourier frequencies around $100\,\text{mHz}$ and $200\,\text{pm}/\sqrt{\text{Hz}}$ at 5 Hz since shortly after launch. A simplified version of the LRI layout is shown in Fig. 1. The racetrack configuration was primarily chosen to circumvent the MWI and cold gas tanks (not shown in Fig. 1) that blocked the line of sight (LOS) between the SC centers of mass (COMs) and, secondly, to minimize tilt-to-length (TTL) coupling from SC attitude jitter. TTL coupling is discussed in detail in Ref. [12] and hence not further explained in this paper.

The LRI operates in an active transponder scheme where the reference SC transmits a frequency-stabilized 1064-nm laser beam to the transponder SC. The laser on the latter is phase-locked to the incoming beam with a 10-MHz frequency offset and sent back to the reference SC where heterodyne interference takes place between the local and the incoming beam to generate a beatnote signal in the megahertz range. The phasemeter extracts the phase of this signal, which is proportional to distance variations

between the SC. The narrow Gaussian beam divergence angle of about $135\,\mu\text{rad}$ makes alignment conditions critical for the interferometer to work since (i) the transmitted (TX) beams have to be aligned to the LOS within the LRI field of view of approximately $\pm100\,\mu\text{rad}$ to deliver enough light to the far SC and (ii) the received (RX) and local beam wave fronts have to be within a similar alignment accuracy on the optical benches to enable interference. The LRI field of view is much narrower than the SC attitude control capabilities, which are about $\pm300\,\mu\text{rad}$ for pitch and yaw, respectively [8]. For this reason, the LRI includes two quadrant photoreceivers (QPRs) [13] that measure the relative angles between the wave fronts of the local and the RX beams through differential wave-front sensing (DWS) [14]. By driving a fast steering mirror (FSM) [15] in a feedback control loop, these signals are kept at zero [16]. With this FSM, the LRI field of regard is approximately $\pm3.5\,\text{mrad}$, limited by the aperture of the baffles. The TX beam propagates through a large retroreflector, the triple mirror assembly (TMA), that ideally maintains the alignment between the RX and TX beams and thus keeps the interferometer geometry in place regardless of the local SC orientation, as is shown in Fig. 1.

Details of the LRI are given in Refs. [7,8], while in this paper, we describe the flight model (FM) assembly process, qualification, and their final characterization in orbit. The requirements, as briefly introduced above, are discussed in more detail in Refs. [7,17,18]. The TMAs were developed as part of the German contribution to the LRI [18]. The detailed design, analysis, manufacturing, qualification, and ground tests of the TMA development, engineering, and flight models were performed by SpaceTech GmbH in collaboration with Hensoldt Optronics GmbH and with contributions from the German Aerospace Centers' Institute of Space Systems and the Max-Planck Institute for Gravitational Physics (Albert-Einstein Institute).

This paper is organized as follows: Sec. II describes the TMA design together with details about its assembly. Section III summarizes the on-ground coalignment measurements at different stages of the mission preparation. In-orbit measurements are described in Sec. IV, which includes the characterization of the transmitted beams after traveling 200 km. A summary of the findings and their impact on future LRI instruments is presented in Sec. V.

II. PROPERTIES AND ASSEMBLY

Retroreflectors hold properties that are invariant under rotation around their vertex point [16,19], which make them ideal for the LRI where significant SC attitude jitter is present. These properties are (i) the propagation path length through the TMA is twice the distance between the beam starting point and a plane orthogonal to the beam direction that intersects the retroreflector vertex, (ii) the direction of the reflected beam is always antiparallel to the

incident beam, and (iii) the lateral beam offset from the axis parallel to the incident beam passing through the vertex is the same for the incident and the reflected beams. Such properties make the TMA a critical component for the LRI, both in functionality and performance. This important role comes with demanding requirements, especially in terms of the so-called coalignment, defined as the angle between the incoming and outgoing beams, which ideally is 180° [20,21]. In practice, the TMA mirrors are not perfectly aligned due to the manufacturing precision and, therefore, introduce a mispointing of the beams traveling between the two spacecraft, reducing the amount of exchanged photons. The pointing requirements regarding the received optical power as well as so-called TTL coupling were studied intensively during the LRI development [20,22] and a beam-pointing offset of 50 µrad was set as a requirement.

The TMA consists of a mechanical frame that provides a stable basis for the mirrors' assemblies. It was developed and assembled by SpaceTech GmbH and Hensoldt Optronics GmbH; the Australian National University developed an alternative TMA, and were involved in testing and concept development for link acquisition. The basic component of the frame is a 430-mm-long, 39-mm-diameter hollow tube with 2 mm thickness made of carbon fiber reinforced plastic (CFRP) that was chosen due to its low coefficient of thermal expansion (CTE) and good stiffness-to-mass ratio. Three mirrors are attached at the ends (one at the input and two at the output) that form a virtual corner cube (or retroreflector) with its virtual vertex at the SC COM—see Figs. 1 and 2. The mirrors' assemblies are made of Zerodur and are responsible for the precision alignment. The hybrid design using CFRP and Zerodur was considered the best compromise between structural strength, thermal stability, and highly stable and accurate alignment in the available space in the SC. The TMA is connected to the accelerometer support plate using a titanium bracket glued to a CFRP bracket, which is, in turn, connected to the tube by means of adapter rings also made of CFRP—see Fig. 2. The mirror assemblies consist of the eight parts shown in Fig. 3: end-fittings 1 and 2, spacer

FIG. 3. Top, smaller images: Zerodur optical parts before their assembly and coating. Bottom: Optical parts of the triple mirror assembly attached to the carbon fiber reinforced plastic tube. See text for details on the assembly procedure.

rings 1 and 2, the three actual mirrors (M1, M2, and M3), and the M2 mount. The mirrors were coated with silver-based broadband highly reflective coating optimized for 1064 nm, which exhibited minimal changes of the light polarization within the TMA field of view.

The assembly procedure of the optical parts began by gluing the Zerodur end-fittings 1 and 2 onto the tube ends. The next step of the assembly consisted of shimming and polishing spacer ring 1 to further improve the position and angle of the end-fitting beyond gluing accuracy. Subsequently, mirror M1 was wringed onto spacer ring 1. Wringing is a technique used to create bonds between two flat polished pieces of glass when they are brought together due to van der Waals forces and allows manipulation of the interface in rotation to achieve the required alignment. Once the alignment is optimized the two pieces are pressed together. The structural strength of the optical contacts was enhanced by including glue pockets in the bonds. In this configuration, the wringed bond provided both precision alignment and stability, while the glue pockets enhanced the mechanical integrity required for the launch loads.

The assembly process continued by wringing the M1/spacer ring 1 onto end-fitting 1 and finally gluing after position adjustment. After this step the TMA tube with end-fitting 1 and M1/spacer ring underwent bake-out. Next, mirrors M2 and M3 were wringed together and onto
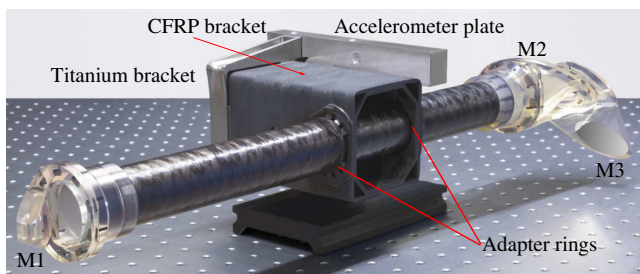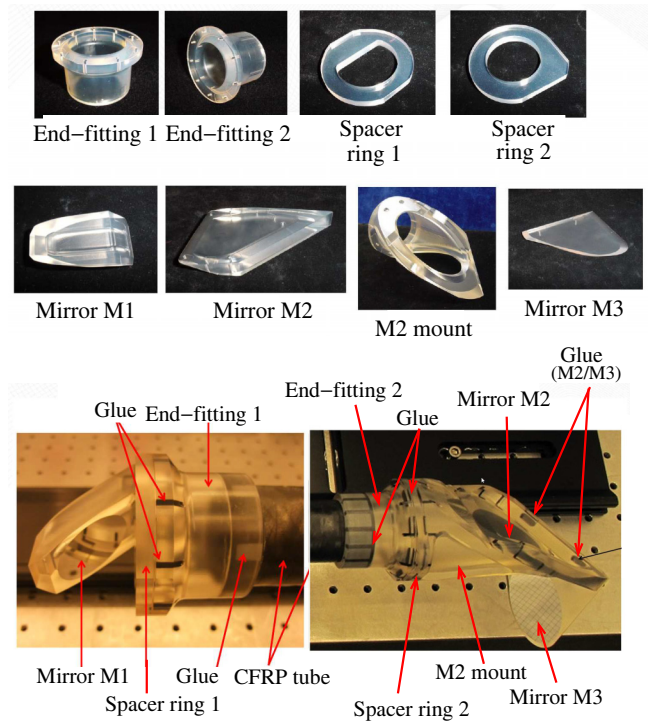

FIG. 2. Photograph of a triple mirror assembly flight model showing the carbon fiber reinforced plastic (CFRP) tube and mounting bracket, as well as the Zerodur glass attachments that hold the three mirrors (M1–M3).

the M2 mount. Spacer ring 2 was then polished to compensate for the errors between end-fitting 2 and the M2/M3 assembly. It was wringed onto end-fitting 2, before the M2 mount, including the M2/M3 mirrors, was wringed to the spacer on end-fitting 2. At this point, the TMA was assembled, but fine adjustment of the coalignment was still possible by rotation of the M2/M3 assembly around end-fitting 2. Once this was accomplished, the glue pockets were filled and the whole TMA baked out. The whole assembly was carried out in a vertical orientation in order to minimize gravity effects, i.e., the CFRP tube was oriented upright such that bending of the tube by the weight of the optical parts was minimized.

III. ON-GROUND MEASUREMENTS

A. Unit level

The TMAs' coalignment at the unit level (after environmental tests: vibration and thermal cycling) was characterized regarding the effect of gravity and its temperature dependency. The measurement setup is shown in Fig. 4 and consisted of a reference flat and an autocollimator (500 mm focal length and 50 mm width, with an accuracy of $\pm 2\,\mu$rad). The reference flat was a block of Zerodur class zero (630 mm in length, 50 mm, and 100 mm in depth) with two surfaces coated in silver that exhibited parallelism of 1 μrad, and was mounted on a 4-degrees-of-freedom Invar athermal mount. The autocollimator measured both the angles (pitch θ and yaw ψ) of a beam passing through the TMA that reflected off the back surface of the reference flat (measurement beam) and the angles of a beam reflected directly off the front surface of the reference flat (reference beam). The measurements were multiplexed by a motorized shutter that blocked alternatively one half of the autocollimator beam at a frequency of 0.1 Hz. The difference between the two measurements provided the actual TMA coalignment as follows:

$$\theta_{\text{TMA}} = \theta_{\text{M}} - \theta_{\text{R}}, \tag{1}$$

$$\psi_{\text{TMA}} = \psi_{\text{M}} - \psi_{\text{R}}, \tag{2}$$

$$\gamma = \sqrt{\theta_{\text{TMA}}^2 + \psi_{\text{TMA}}^2}, \tag{3}$$

where the subscripts M and R stand for measurement and reference beams, respectively. Equation (3) provides the coalignment error in terms of a half-cone angle.

The coalignment error γ after assembly of the flight model versions was around 10 μrad. It was subsequently measured in horizontal and vertical orientations, i.e., under 1g and 0g conditions, in vacuum, and at different temperatures. For measuring the influence of gravity, the autocollimator, reference flat, and the TMA were mounted on a rotating table to mimic 0g conditions. Both TMA flight models behaved very similarly and in good agreement with
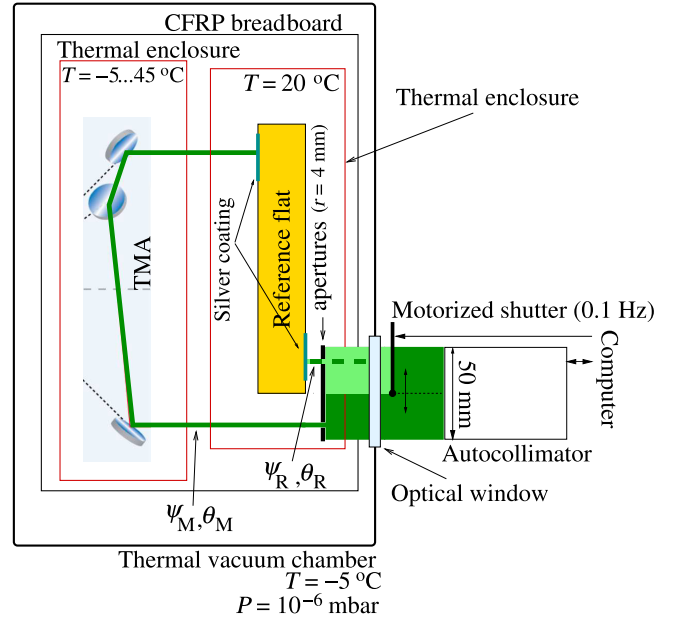

FIG. 4. Coalignment measurement laboratory setup. The autocollimator measured the angle of a beam going through the triple mirror assembly and reflected off the back surface of the reference flat (dark green) and a beam reflected directly from the reference flat (light green, dashed). The beams were multiplexed every 10 s using a motorized shutter. CFRP, carbon fiber reinforced plastic.

simulations. The results for both of them were

$$\Delta\theta = \theta_{0g} - \theta_{1g} = +50 \pm 2\,\mu\text{rad}, \tag{4}$$

$$\Delta\psi = \psi_{0g} - \psi_{1g} = +5 \pm 2\,\mu\text{rad}. \tag{5}$$

All the following measurements are corrected by these values in order to always compare the coalignment in its 0g state.

For the environmental tests, the TMA and the reference flat were placed inside a thermal vacuum chamber (TVC) in two independent housings with heaters. The reference flat was kept at 20 °C, while the TMA temperature was changed from 5 to 35 °C. The setup was highly insensitive to common tilts coming from, e.g., the autocollimator, the TVC, the optical window, or the reference flat, since they canceled out when taking the difference between the reference and measurement beams. The results are shown in Fig. 5. The colored traces are coalignment values at different temperatures in vacuum. The black dots represent the measurements where the temperature of the TMA had homogenized and reached a steady-state condition. The dashed circle indicates the 50-μrad requirement. The bottom panels show the pitch and yaw angles as a function of temperature. The dashed square indicates the coalignment requirement within the LRI temperature range. Both TMAs met the requirements for almost the entire expected temperature range. However, the coalignment exhibited
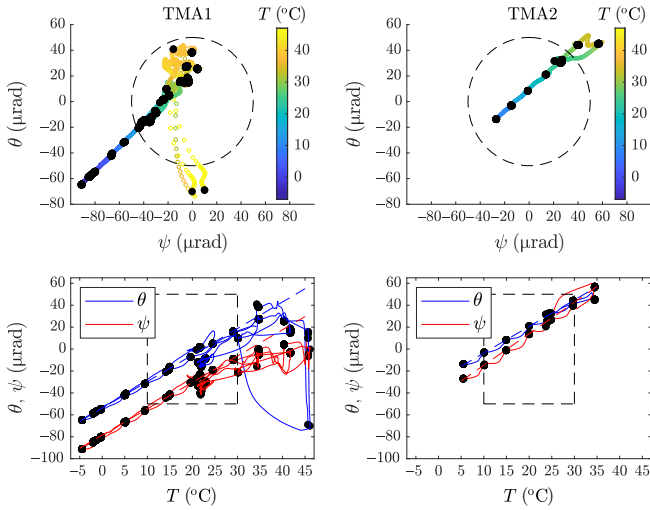
FIG. 5. Coalignment for triple mirror assembly 1 (TMA1) (left) and TMA2 (right) in unit-level tests. TMA1 was tested from -5 to $45\,^\circ$C to examine nonlinear behavior beyond the laser ranging interferometer temperature range. Top figures: Polar coordinates. Colors indicate the temperature from cold (blue) to warm (yellow). The dashed circle indicates the 50-μrad half-cone angle requirement. Bottom figures: Pitch and yaw coalignment errors as a function of temperature. The dashed square represents the requirement in the LRI temperature range. Black dots correspond to values where the TMA temperature had reached a steady-state condition.

a nonlinear behavior around $30\,^\circ$C that caused sudden changes of tens of microradians. In order to better observe this behavior, the testing temperature range for TMA1 was extended to -5 to $45\,^\circ$C. A sudden change of -90 μrad in pitch was observed at $45\,^\circ$C, which vanished while returning to room temperature. The coalignment in yaw was much less sensitive to temperature but still exhibited a nonlinear behavior above $30\,^\circ$C. At the low-temperature end, there was no sign of nonlinearity. The reason behind the sudden changes at high temperatures was attributed to the thermal expansion of the glue in the pockets used to strengthen the optical bonds between mirrors. Nevertheless, in the LRI temperature range, 10 to $30\,^\circ$C, the coalignment behaved linearly and, thus, was modeled as

$$\theta(T) = a_\theta(T - T_0) + b_\theta, \tag{6}$$

$$\psi(T) = a_\psi(T - T_0) + b_\psi, \tag{7}$$

where $T_0 = 20\,^\circ$C. The fitted temperature coefficients were $+2.4$ μrad/K for pitch and yaw on TMA1 as well as for pitch on TMA2, and $+2.9$ μrad/K for yaw on TMA2—see Table I.

The coalignment values between the TVC campaign and the $0g$ tests shifted by 34 μrad and 51 μrad in pitch and yaw in TMA1 and 19 μrad and 3 μrad in TMA2 compared to the previous measurements in vacuum. The half-cone angles γ in April 2015 were 26 μrad and 43 μrad

TABLE I. Unit-level TMA coalignment values b at $20\,^\circ$C and temperature coefficients a measured in the thermal vacuum chamber.

	a_θ (μrad/K)	b_θ (μrad)	a_ψ (μrad/K)	b_ψ (μrad)
TMA1	$+2.4$	-5	$+2.4$	-30
TMA2	$+2.4$	$+21$	$+2.9$	$+14$

in TMA1 and TMA2, respectively. The coalignment shifts were attributed to moisture accumulation on the CFRP tube and/or the mirrors' glue pockets over the time elapsed since the last measurements, 6 months for TMA1 and 2 months for TMA2—see the Supplemental Material [23].

B. Spacecraft level

Coalignment measurements were taken recurrently at the SC level to ensure that the TMAs remained functional and within the requirements. First, the TMAs were installed on a large breadboard to simulate the SC platform and allow for the installation of all the LRI subsystems together for the first time. The coalignment measurements in such configuration showed changes of 8 μrad and 14 μrad in pitch and yaw in TMA1, and of 11 μrad and 28 μrad in TMA2 compared with previous measurements.

After that breadboard test, the LRI subsystems were delivered and assembled onto the SC at the Airbus facilities and, shortly after, coalignment measurements took place for the first time at the SC level. TMA1 had changed by -8 μrad and -25 μrad in pitch and yaw, respectively. TMA2 had changed by -12 μrad in yaw only. The half-cone angles, after integration on the SC, were 21 μrad and 61 μrad for TMA1 and TMA2, respectively.

The next step consisted of shipping the SC to IABG in Ottobrunn, Germany, for environmental tests (thermal vacuum cycling, sine vibration, acoustic tests, electromagnetic compatibility tests, etc.). SC-1 went to thermal vacuum cycling first and, subsequently, its coalignment was measured. The results showed almost no difference from the previous ones at Airbus. From February 2017 to August 2017, SC-1 went through acoustic and sine vibration testing while SC-2 went through thermal vacuum, acoustic, and sine vibration testing without the possibility of coalignment measurements in between. The next measurement was again on SC-1 in August 2017, and it exhibited a large coalignment error in pitch, $\theta = -126$ μrad, that resembled the large jump observed at $45\,^\circ$C in the unit-level tests. Such coalignment was close to the maximum allowed for the LRI to work in nominal conditions, 150 μrad, and above the maximum value in worst-case scenario conditions, 105 μrad. Moreover, it raised concerns about the mechanical integrity of the TMA, which could not be assessed directly since it was now inaccessible inside the SC. The presumed reason behind this large misalignment was the same one stated during unit-level

tests: the expanding glue in the pockets slightly loosened the optical bonds in the mirror assemblies and thus dominated the TMA coalignment. In this case, instead of the glue's thermal expansion, the cause was moisture accumulation over time. The idea was supported by visual inspection on the spare flight and engineering models that were found to exhibit loss of optical contact in several bonds. TMA2's half-cone angle after SC environmental tests increased from 61 to 83 μrad. TMA1 was measured again under different orientations (by rotating the whole SC) in order to assess whether the $1g$ to $0g$ correction was still valid. The results for the corrections were identical to the ones measured at the unit level. By the end of 2017, 5 months before launch, the coalignment values γ were 132 μrad for TMA1 and 94 μrad for TMA2. While TMA1 had gone through a large "sudden" coalignment shift, TMA2 had slowly accumulated coalignment errors over time.

In view of these developments, it is important to note that the TMA glue pockets have been designed to survive the launch loads on their own for the very reason that was now observed: A potential loss of optical bond during launch, e.g., due to shock loads, required that the glue contact would ensure the structural integrity of the TMA. This turned out to be a good engineering decision, although the effect of moisture intake and glue expansion over the years-long assembly, integration, and test process had not been foreseen at that time. However, as now the "potential case" became the nominal launch case, a series of additional rigorous tests were performed on the TMA qualification model, flight spare, development model, and test samples, including qualification-level vibration tests and destructive pull tests. Furthermore, in vacuum tests on the qualification model and flight spare, it was verified that within about 8 weeks in vacuum, the coalignment was restored to the original levels, supporting the hypothesis of moisture-related glue expansion. In parallel, measures to fly the LRI with a DWS offset to compensate for larger coalignment errors were investigated with a positive outcome. With these results verifying the safety and in-orbit performance, the TMAs were cleared for launch.

Next, the SC were shipped to the launch site at the Vandenberg Air Force Base (VAFB) in California. Coalignment was measured again, and small discrepancies were observed from the previous results in Germany. Three months before launch, the SC were moved to the spaceport operations Harris near the Space Launch Complex 6 at the VAFB. The last measurements took place on March 14, 2018, and were consistent with the previous ones: 120 μrad and 81 μrad for TMA1 and TMA2, respectively. Finally, the coalignment temperature coefficients were also estimated at the VAFB site. This was done by measuring the coalignment while switching on SC subsystems, which caused a TMA temperature increase of 5 K. For TMA1, the pitch and yaw coefficients were −3.5 μrad/K and

4.9 μrad/K, i.e., significantly larger than the ones at the unit level and with a reversed sign in pitch—see Table I. The negative pitch coefficient resembled the one at the unit level when returning to room temperature after the excursion to 45 °C—see Fig. 5 (bottom left). This again supports the root cause analysis that the TMA was in a similar state as in earlier high-temperature measurements, although this time driven by moisture accumulation in the glue pockets instead of thermal expansion. It reaffirmed that, after launch, the coalignment would slowly recover.

Fortunately, the LRI performance in orbit and dedicated coalignment measurements described below confirmed this.

IV. IN-ORBIT MEASUREMENTS

After a successful initial laser-link acquisition scan [24–26], the LRI entered science mode on June 14, 2018, on the first attempt, meaning that the interferometric link was established, and ranging data were collected. The recorded carrier-to-noise density ratio C/N_0 was approximately 88 dB − Hz in both SC [8], which was close to the expected maximum and indicates good alignment of the optical bench, but also a low TMA coalignment error, which was further confirmed by the measurements described in Refs. [26–28] and the following.

In nominal operations, the DWS signal in the pitch and yaw angles is zeroed by the steering mirror control loop to ensure the alignment between the incoming and outgoing beams on both spacecraft. By commanding nonzero setpoints to the DWS, the pointing of the locally transmitted beam is altered. As discussed already in Sec. II, this mispointing reduced the received beam power on the distant spacecraft. Commanding the DWS setpoints in a pattern allows mapping of the far-field intensity of the transmitted laser beam alongside some more beam parameters [28].

Let $P_{\mathrm{RX},i}$ be the received light power at the distant spacecraft SC-i. It is measured through the interferometric beatnote amplitude, which is calculated from the digital phase-lock loop (DPLL) running in the phasemeter as

$$\mathcal{A}_{\mathrm{BN}} = \sqrt{\mathcal{I}^2 + \mathcal{Q}^2}/k \simeq \mathcal{I}/k, \qquad (8)$$

where $\mathcal{I}$ and $\mathcal{Q}$ are the in-phase and quadrature components of the beatnote, respectively. The latter is kept at zero by the DPLL. k accounts for gains in the measurement chain. The beatnote amplitude $\mathcal{A}_{\mathrm{BN}}$ corresponds to the coherent sum of the four quadrants of both QPRs, i.e.,

$$\mathcal{A}_{\mathrm{BN}}^2 = 4\mathcal{R}^2\eta_{\mathrm{het}}\eta_{\mathrm{BS}}^{\mathrm{t}}P_{\mathrm{laser}}\eta_{\mathrm{BS}}^{\mathrm{r}}P_{\mathrm{RX}} \simeq (\mathcal{I}/k)^2, \qquad (9)$$

where P_{RX} is the received power at the distant spacecraft, $\eta_{\mathrm{BS}}^{\mathrm{r\,(t)}}$ is the reflectivity (transmissivity) of the beam splitter, and η_{het} the heterodyne efficiency—see, e.g., Ref. [22]. Notice that all the terms in Eq. (9) are constant over short

time scales (a few hundred seconds) in nominal operations, but the received power $P_{\text{RX},i}$ varies on introducing DWS offsets in SC-j. For an elliptical Gaussian beam and non-ideal TMA in SC-j, the normalized received power in SC-i can be expressed as

$$P_{\text{RX},i}^{\text{model}} = \mathcal{A}_i^2 \exp\left\{ -\left[\frac{(\theta_j - \theta_j^0)\cos\vartheta_j + (\psi_j - \psi_j^0)\sin\vartheta_j}{\Theta_j^a} \right]^2 - \left[\frac{-(\theta_j - \theta_j^0)\sin\vartheta_j + (\psi_j - \psi_j^0)\cos\vartheta_j}{\Theta_j^b} \right]^2 \right\}.$$

(10)

where θ_j and ψ_j are the beam-pointing offsets introduced on SC-j. θ_j^0 and ψ_j^0 are the offsets at which the received power in SC-i is the highest and they approximately correspond to the TMA coalignment error in SC-j with the sign inverted. ϑ_j is the rotation of the principal beam axis leaving SC-j, i.e., the ellipse semi-axes with respect to the LRI optical frame. $\Theta_j^{a,b}$ are the divergence angles of the beam leaving SC-j within that rotated frame.

The measured data are, on the one hand, the squared amplitude of the beatnote on SC-i, $\mathcal{A}_i^2$, and, on the other hand, the beam-pointing offsets introduced on SC-j. The free parameters in the model $\{\mathcal{A}_i, \theta_j^0, \psi_j^0, \Theta_j^a, \Theta_j^b, \vartheta_j\}$ are estimated by minimizing the sum of squared residuals χ^2 defined as

$$\chi^2 = \sum_{\theta_j, \psi_j} (P_{\text{RX},i}^{\text{model}} - \mathcal{A}_i^2)^2,$$

(11)

with $(i = 2, j = 1)$ and $(i = 1, j = 2)$ for characterizing the transmitted beams of SC-1 and SC-2, respectively.

The first in-orbit coalignment measurement took place on June 18, 2018, during the LRI commissioning phase. The DWS offset pattern applied in SC-1 is shown in Fig. 6 (left panel). It consisted of a 168-point spiral pattern and
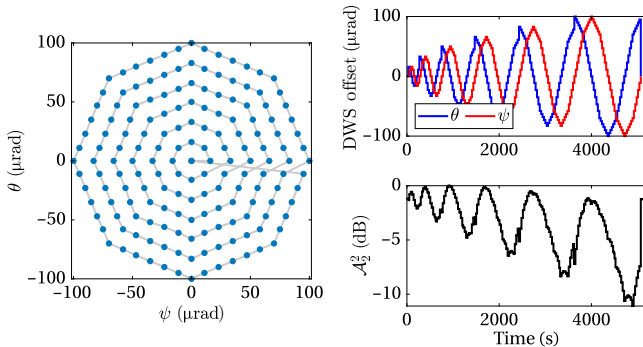

FIG. 6. Left: Differential wave-front sensing (DWS) offset pattern applied on spacecraft 1 (SC-1). Top right: DWS offset pattern as a function of time. Bottom right: Squared and normalized beatnote amplitude in SC-2, $\mathcal{A}_2^2$, for the DWS scan in July 2018.
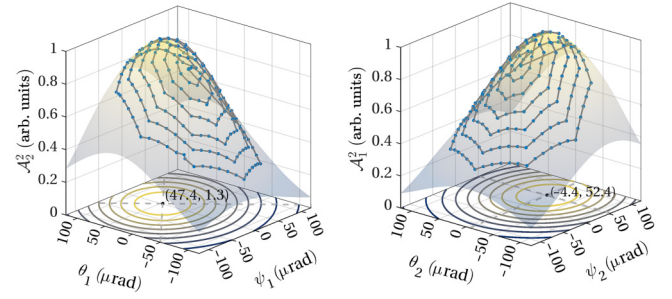

FIG. 7. Power $\mathcal{A}_i^2$ received on SC-i as a function of the misalignment of the SC-j beam: measured data (dots) and fit (bell shape) for the characterization of both beams in July 2018. The written numbers denote the differential wave-front sensing offset angles (θ_j^0, ψ_j^0) on SC-j at the maximum received power on SC-i. These offsets are needed to compensate the triple mirror assembly coalignment error. Left: SC-1 scanning ($i = 2, j = 1$). Right: SC-2 scanning ($i = 1, j = 2$).

took 85 min for each SC to execute. The top right panel shows the time evolution of the DWS offsets, and the bottom right one shows the corresponding beatnote amplitude $\mathcal{A}_2^2$ recorded on SC-2 throughout the scan.

The received power on SC-2 as a function of the DWS offsets in SC-1 and the corresponding fit are shown in Fig. 7 (left), which shows the intensity distribution of the Gaussian beam leaving SC-1 after traveling 215 km. This measurement revealed a TMA1 coalignment error of $-47.4 \pm 16.8\,\mu\text{rad}$ and $-1.3 \pm 13.6\,\mu\text{rad}$ for pitch and yaw, respectively. Similarly, the right panel of Fig. 7 reveals a TMA2 coalignment error of $-4.4 \pm 9.8\,\mu\text{rad}$ and $52.4 \pm 16.6\,\mu\text{rad}$ in pitch and yaw, respectively. The time evolution of these coalignment errors is shown in Fig. 8 over the green background color for the in-orbit period. Table S1 in the Supplemental Material [23] shows all the fit parameters. It is observed that the coalignment error almost vanishes after some time in orbit and stays close to zero.

The Gaussian beam parameters, which have been coestimated alongside the TMA coalignment errors, exhibited divergence angles between 124 and 146 μrad in both axes on both SC. The time evolution of the divergence angles, shown in Table S2 and Fig. S1 in the Supplemental Material [23], shows that the spatial properties of the Gaussian beams exchanged are fairly stable.

The temperature susceptibility of the coalignment was also roughly estimated from the in-orbit measurements. The results for TMA1 are $-0.3 \pm 0.5\,\mu\text{rad/K}$ and $-2.0 \pm 2.7\,\mu\text{rad/K}$ for pitch and yaw, respectively. The values for TMA2 are $1.1 \pm 0.1\,\mu\text{rad/K}$ and $-2.3 \pm 0.6\,\mu\text{rad/K}$ for pitch and yaw, respectively. These results are significantly smaller than the ones measured just before launch and thus confirm that they were mostly driven by the glue due to moisture accumulation. More information can be found in Ref. [28].
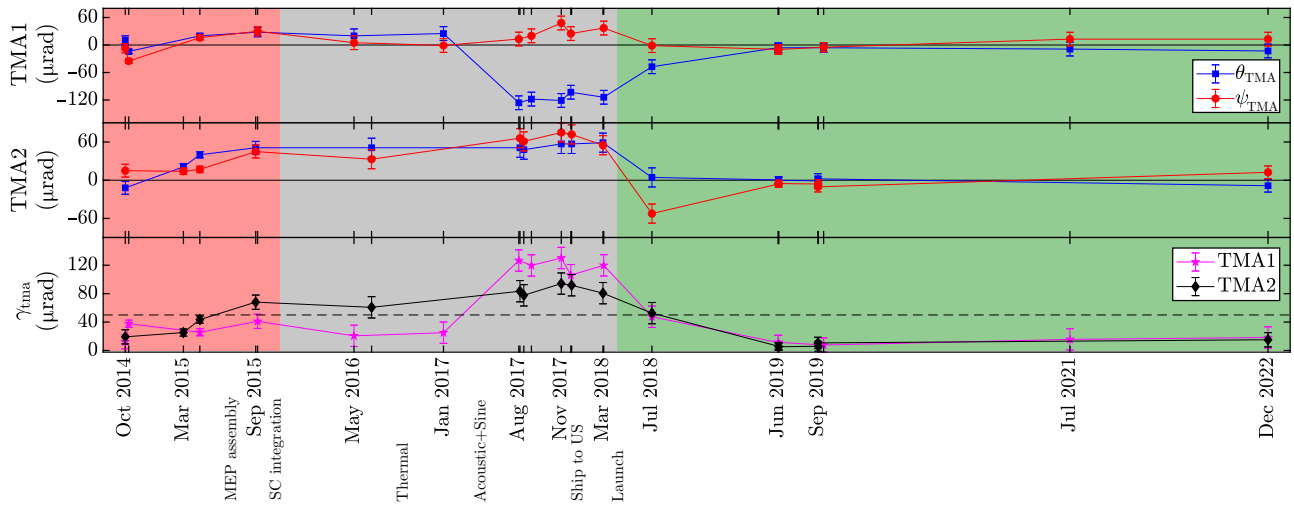
FIG. 8.   Summary of the triple mirror assembly (TMA) mirror coalignment measurements. Top: Pitch and yaw for TMA1. Center: Pitch and yaw for TMA2. Bottom: Half-cone angle γ, for TMA1 and TMA2. The dashed black trace is the 50-μrad requirement. The red background denotes the characterization at the unit level, gray denotes the spacecraft level (after integration of the TMAs into the spacecraft), and green are in-orbit measurements. MEP, main equipment platform.

V. SUMMARY

This paper discussed the design, construction, and testing of large cornercube-like retroreflectors for the inter-spacecraft laser ranging interferometer, called the triple mirror assemblies. The major challenge was the narrow requirement on the mirror coalignment. Figure 8 summarizes the coalignment error measurements of the two TMA flight models from their assemblies in 2014 to the latest in-orbit measurements in late 2022.

The initial coalignment errors were at the 10-μrad level but slowly changed over time and reached values of 120 and 80 μrad for TMA1 and TMA2 shortly before launch, far beyond the requirement. The reason behind this coalignment degradation over time was the expansion of the glue pockets in the Zerodur mirrors' assemblies due to moisture accumulation. However, the LRI was able to acquire the laser link at the first try, and subsequent in-orbit measurements showed the TMAs' coalignment slowly recovered while the accumulated moisture outgassed until a near-perfect alignment was exhibited after one year in space, as predicted from on-ground coalignment characterization.

The in-orbit coalignment measurements also provided the far-field intensity distribution of the Gaussian beams exchanged between the SC after traveling approximately 200 km and allowed us to estimate the beams' divergence angles. The results showed slightly elliptical beams with a few percent larger divergence angles than the ones measured during on-ground testing. The exact values for all ground and in-flight coalignment measurements are given in Table S1 in the Supplemental Material [23], while Table S2 provides the estimated Gaussian beam parameters for the in-orbit measurements.

The next generation of gravity field missions will fully rely on laser interferometry for the intersatellite ranging, given its superb sensitivity and rather small size, weight, and power requirements. More specifically, the upcoming GRACE-C and NGGM missions will fly the laser interferometer with the GRACE Follow-On racetrack design as the main instrument, with increased redundancy to meet the reliability requirements. As for the TMA, the issues addressed in detail in this paper have been solved by an updated design of the glue-strengthened optical bonds, which does not lead to the observed decontacting under moisture and temperature while maintaining the alignment accuracy, stability, and (relatively) easy assembly of the units. More specifically, different glue pocket geometries and different adhesives have been investigated and thoroughly tested over temperature, humidity, and long-term behavior. In this investigation, the shortcomings of the original design could be reproduced on representative sample pieces, and working solutions have been identified. Ultimately, a different adhesive, which is cured at a higher temperature and has lower coefficient of moisture expansion and CTE, together expanding the usable temperature range, is now applied and will be flown after successful qualification.

DATA AVAILABILITY

Some of the data that support the findings of this article are openly available [29]. Data underlying the results presented in this paper for the on-ground campaigns are not publicly available. The data are available from the authors upon reasonable request.

[1] B. D. Tapley, S. Bettadpur, J. C. Ries, P. F. Thompson, and M. M. Watkins, GRACE measurements of mass variability in the Earth system, Science **305,** 503 (2004).

[2] J. Wahr, S. Swenson, V. Zlotnicki, and I. Velicogna, Time-variable gravity from GRACE: First results, Geophys. Res. Lett. **31** (2004).

[3] R. P. Kornfeld, B. W. Arnold, M. A. Gross, N. T. Dahya, W. M. Klipstein, P. F. Gath, and S. Bettadpur, GRACE-FO: The Gravity Recovery and Climate Experiment Follow-On mission, J. Spacecr. Rockets **56,** 931 (2019).

[4] F. W. Landerer *et al.*, Extending the global mass change data record: GRACE Follow-On instrument and science data performance, Geophys. Res. Lett. **47,** e2020GL088306 (2020).

[5] C. Dunn, W. Bertiger, Y. Bar-Sever, S. Desai, B. Haines, D. Kuang, F. Garth, I. Harris, G. Kruizinga, T. Meehan, S. Nandi, D. Nguyen, T. Brooks, J. Brooks Thomas, J. Tien, L. Romans, M. Watkins, S.-C. Wu, S. Bettadpur, and J. Kim, Instrument of GRACE: GPS augments gravity measurements (2003).

[6] F. Flechtner, P. Morton, M. Watkins, and F. Webb, in *Gravity, Geoid and Height Systems*, edited by U. Marti (Springer International Publishing, Cham, 2014), p. 117.

[7] B. S. Sheard, G. Heinzel, K. Danzmann, D. A. Shaddock, W. M. Klipstein, and W. M. Folkner, Intersatellite laser ranging instrument for the GRACE Follow-On mission, J. Geod. **86,** 1083 (2012).

[8] K. Abich *et al.*, In-orbit performance of the GRACE Follow-On laser ranging interferometer, Phys. Rev. Lett. **123,** 031101 (2019).

[9] D. Wiese, B. Bienstock, D. Bearden, C. Boening, K. Case, J. Chrone, S. Horner, B. Loomis, S. Luthcke, M. Rodell, J. Sauber, L. Tsaoussi, F. Webb, and V. Zlotnicki, *The NASA Mass Change Designated Observable Study: Progress and Future Plans, EGU General Assembly 2021*, online, 19–30 Apr 2021, EGU21-8088 (2021).

[10] K. Nicklaus, K. Voss, A. Feiri, M. Kaufer, C. Dahl, M. Herding, B. A. Curzadd, A. Baatzsch, J. Flock, M. Weller, V. Müller, G. Heinzel, M. Misfeldt, and J. J. E. Delgado, Towards NGGM: Laser tracking instrument for the next generation of gravity missions, Remote Sens. **14,** 4089 (2022).

[11] P. Amaro-Seoane *et al.*, Laser interferometer space antenna, ArXiv:1702.00786.

[12] H. Wegener, V. Müller, G. Heinzel, and M. Misfeldt, Tilt-to-length coupling in the GRACE Follow-On laser ranging interferometer, J. Spacecr. Rockets **57,** 1362 (2020).

[13] G. F. Barranco, O. Gerberding, T. S. Schwarze, B. S. Sheard, C. Dahl, B. Zender, and G. Heinzel, Phase stability of photoreceivers in intersatellite laser interferometers, Opt. Express **25,** 7999 (2017).

[14] E. Morrison, B. J. Meers, D. I. Robertson, and H. Ward, Automatic alignment of optical interferometers, Appl. Opt. **33,** 5041 (1994).

[15] H. Langenbach, and M. Schmid, in *11th European Space Mechanisms and Tribology Symposium, ESMATS 2005*, ESA Special Publication, Vol. 591, edited by B. Warmbein (ESA, 2005), p. 27.

[16] D. Schütze, G. Stede, V. Müller, O. Gerberding, T. Bandikova, B. S. Sheard, G. Heinzel, and K. Danzmann, Laser beam steering for GRACE Follow-On intersatellite interferometry, Opt. Express **22,** 24117 (2014).

[17] D. Schütze, V. Müller, G. Stede, B. S. Sheard, G. Heinzel, K. Danzmann, A. J. Sutton, and D. A. Shaddock, Retro-flector for GRACE Follow-On: Vertex vs. point of minimal coupling, Opt. Express **22,** 9324 (2014).

[18] K. Abich, C. Bogan, C. Braxmaier, K. Danzmann, M. Dehne, M. Gohlke, A. Görth, G. Heinzel, M. Herding, C. Mahrdt, V. Müller, K. Nicklaus, J. Sanjuan, D. Schütze, B. Sheard, G. Stede, and K. Voss, GRACE-Follow On laser ranging interferometer: German contribution, J. Phys.: Conf. Ser. **610,** 012010 (2015).

[19] R. L. Ward *et al.*, The design and construction of a prototype lateral-transfer retro-reflector for inter-satellite laser ranging, Classical Quantum Gravity **31,** 095015 (2014).

[20] D. Schütze, D. Farrant, D. A. Shaddock, B. S. Sheard, G. Heinzel, and K. Danzmann, Measuring coalignment of retroreflectors with large lateral incoming-outgoing beam offset, Rev. Sci. Instrum. **85,** 035103 (2014).

[21] R. Fleddermann *et al.*, Testing the GRACE Follow-On triple mirror assembly, Classical Quantum Gravity **31,** 195004 (2014).

[22] C. Mahrdt, *Laser link acquisition for the GRACE Follow-on laser ranging interferometer*, Ph.D. thesis, Gottfried Wilhelm Leibniz Universität, Hannover, 2014.

[23] See Supplemental Material at http://link.aps.org/supplemental/10.1103/7ps8-317c for all TMA mirror coalignment measurements from the unit level to in-flight measurements for both TMA flight units.

[24] A. Koch, J. Sanjuan, M. Gohlke, C. Mahrdt, N. Brause, C. Braxmaier, and G. Heinzel, Line of sight calibration for the laser ranging interferometer on-board the GRACE Follow-On mission: on-ground experimental validation, Opt. Express **26,** 25892 (2018).

[25] D. M. R. Wuchenich, C. Mahrdt, B. S. Sheard, S. P. Francis, R. E. Spero, J. Miller, C. M. Mow-Lowry, R. L. Ward, W. M. Klipstein, G. Heinzel, K. Danzmann, D. E. McClelland, and D. A. Shaddock, Laser link acquisition demonstration for the GRACE Follow-On mission, Opt. Express **22,** 11351 (2014).

[26] A. Koch, *Link acquisition and optimization for intersatellite laser interferometry*, Ph.D. thesis, Gottfried Wilhelm Leibniz Universität, 2020.

[27] M. Misfeldt, *Data Processing and Investigations for the GRACE Follow-On Laser Ranging Interferometer*, Masters' Thesis, Leibniz Universität Hannover, 2019.

[28] M. Misfeldt, *In-Depth Characterization of the First Inter-Satellite Laser Ranging Interferometer on GRACE Follow-On*, Ph.D. thesis, QUEST Leibniz Forschungsschule, Leibniz Universität Hannover, 2023.

[29] Information System and Data Center by the GFZ Helmholtz Centre for Geoscience, https://isdc.gfz-potsdam.de/grace-fo-isdc/ (accessed: 19.12.2024).